JGR Oceans

RESEARCH ARTICLE
10.1029/2019JC015700

Late-1980s Regime Shift in the Formation of the North Pacific Subtropical Mode Water

Sang-Yeob Kim[1], Gyundo Pak[2], Ho Jin Lee[1,3], Young-Oh Kwon[4], and Young Ho Kim[5]

[1]Ocean Science and Technology School, Korea Maritime and Ocean University, Busan, South Korea, [2]Ocean Circulation and Climate Research Center, Korea Institute of Ocean Science and Technology, Busan, South Korea, [3]Department of Ocean Science, Korea Maritime and Ocean University, Busan, South Korea, [4]Woods Hole Oceanographic Institution, Woods Hole, MA, USA, [5]Department of Oceanography, Pukyong National University, Busan, South Korea

Key Points:
- The air-sea interaction primarily drives the formation of the North Pacific subtropical mode water prior to late-1980s
- Since late-1980s, the formation of the subtropical mode water is mainly controlled by the ocean dynamics driven by remote forcing
- The variability of the formation rate is associated to the North Pacific Oscillation

Correspondence to:
H. J. Lee,hjlee@kmou.ac.kr

Citation:
Kim, S.-Y., Pak, G., Lee, H. J., Kwon, Y.-O., & Kim, Y. H. (2020). Late-1980s regime shift in the formation of the North Pacific subtropical mode water. *Journal of Geophysical Research: Oceans*, *125*, e2019JC015700. https://doi.org/10.1029/2019JC015700

Received 26 SEP 2019
Accepted 4 FEB 2020
Accepted article online 7 FEB 2020

Abstract The formation mechanism as well as its temporal change of the North Pacific subtropical mode water (NPSTMW) is investigated using a 50-year (1960–2009) ocean general circulation model hindcast. The volume budget analysis suggests that the formation of the NPSTMW is mainly controlled by the air-sea interaction and ocean dynamics, but there is a regime shift of the relative importance between the two around late-1980s. While the local air-sea interaction process is a main driver of the NPSTMW formation prior to late-1980s, ocean dynamics including the vertical entrainment become dominant since then. The NPSTMW formation is affected by the North Pacific Oscillation simultaneously in the early period, but with a few years lag in the later period. The interdecadal change of the driving mechanism of the interannual variability of the NPSTMW is probably due to the stronger (weaker) influence of local atmospheric forcing in the western North Pacific and unfavorable (favorable) wind stress curl condition for the remote oceanic forcing from the central North Pacific during the former (later) period. This regime shift may be related to the change of centers of the actions of the wind stress curl since the late-1980s.

Plain Language Summary Using a three-dimensional ocean model, we conduct a numerical simulation for 1960–2009. The ocean model reproduces well the feature of the North Pacific subtropical mode water (NPSTMW), which is characterized by a thick subsurface layer of the relatively uniform temperature and potential density, to the east and south of Japan. During cooling seasons (from December to following March), the NPSTMW is formed by the atmospheric cooling and the oceanic processes, such as the deepening of the mixed layer depth and advective flux. Our study found that the relative contributions from the two factors differ in two different epochs, before and after late-1980s. Before late-1980s, the atmospheric cooling mainly controls the NPSTMW formation, while the oceanic processes driven by remote forcing significantly contribute the NPSTMW formation after late-1980s. The variability of the NPSTMW formation is related to the basin-scale climate variability, particularly the North Pacific Oscillation.

1. Introduction

The North Pacific subtropical mode water (NPSTMW), which is characterized by a thick subsurface layer of the relatively uniform temperature (16–20 °C) and potential density (σ_θ = 24.8–25.7 kg m^{-3}) as well as low potential vorticity (PV), is found in the Kuroshio Extension (KE) region (Masuzawa, 1969; Oka & Qiu, 2012). The NPSTMW affects sea surface temperature (SST), geochemical tracers, and subtropical counter current. The NPSTMW subducts into the thermocline with the memory of wintertime SST and reemerges to the surface in the following winter to affect upper-layer distribution of nutrient and the oceanic uptake of the carbon dioxide (Bates, 2012; Oka et al., 2019). In addition, the meridional position of the subtropical counter current is maintained by the horizontal distribution of the NPSTMW (Kobashi et al., 2006), which means that the NPSTMW can affect the oceanic circulation. Therefore, the NPSTMW can be a good indicator for oceanic conditions of the North Pacific.

Previous studies suggested two different main factors driving the interannual variation of the NPSTMW formation: (1) the ocean mixed layer thermodynamics driven by local air-sea buoyancy flux and (2) the ocean dynamics driven by remote atmospheric wind forcing or local ocean current instability. Hanawa (1987) showed that the NPSTMW is formed at the outcrop area of the SST 16–19 °C zone by a large oceanic heat loss during the cooling season using the hydrographic data from 1970 to 1985. Hanawa and Hoshino

©2020. American Geophysical Union. All Rights Reserved.

(1988) suggested that the air-sea heat transfer is closely related to the formation of the NPSTMW during wintertime from the 10 stations observation data along the section at the south of Japan during 1964–1986. Bingham (1992) also reported that the formation of the NPSTMW has close relationships with the amount of oceanic heat release due to the local atmospheric cooling in winter using the hydrographic data obtained from a few number of stations and the expendable bathythermograph data during 1977–1984. Meanwhile, there are two types of oceanic control on the NPSTMW formation (Qiu & Chen, 2006). One is pycnocline depth anomalies that have propagated from the east and determine the stratification in the NPSTMW formation area. Cerovečki and Giglio (2016) suggested that the interannual variability of the volume and density of the NPSTMW, using the Argo data during 2005–2012, is affected by the PV anomaly carried by the westward propagating Rossby waves from the basin-scale climate variability. The other is the resultant changes of eddy activity in the KE region that further modulates the stratification in the NPSTMW formation region. Qiu and Chen (2006) found that the NPSTMW formation is increased (reduced) when the KE is stable (unstable), based on the analysis of the observational data during 1993–2004. However, these studies do not reveal the long-term variability of the NPSTMW formation due to the limitations of the temporal and spatial observational data.

Meanwhile, there are studies reporting the epoch-dependent forcing mechanism on the winter upper-layer thermal states in the western North Pacific, based on the basin-scale long-term data or model simulations. According to the previous studies (Pak et al., 2014, 2019; Park et al., 2012), the East-Asia winter monsoon (EAWM) had a greater influence on the winter SST variability in the western North Pacific compared to the influence of the ocean dynamics before 1990, whereas the opposite is true after 1990. Sugimoto and Kako (2016) reported that the thermocline change due to the Rossby wave propagation is a main controlling factor for the winter mixed layer depth (MLD) and core-layer temperature of summer NPSTMW in the KE region after late-1980s, while it is the surface heat flux during 1970s–1980s. These researches commonly suggested that a regime shift of driving factors for the interannual variability of the winter upper-ocean thermal state near the KE occurred around late-1980s. Because the NPSTMW is highly dependent on the upper-layer thermal states, the same change may exist in the formation of the NPSTMW. However, a recent study by Oka et al. (2019) reported that the variation of the NPSTMW volume is primarily controlled by a remote forcing related with the Pacific Decadal Oscillation with a time lag of 3–4 years using the hydrographic data along the 137°E section from 1967 to 2016. Therefore, the primary driving mechanism for the NPSTMW formation and its potential nonstationarity is yet to be clarified. The purpose of this study is to investigate whether there is an epoch-dependent change in driving mechanism of the NPSTMW formation using a long-term eddy-permitting ocean general circulation model (OGCM) results forced by the interannual atmospheric forcing. The use of OGCM results will complement the previous studies based on the limited observational data in the study region. We should note that we did not consider the local eddy effect suggested by Qiu and Chen (2006) in this study, because the eddy activity in the KE region cannot be reproduced realistically in the eddy-permitting model.

This paper is organized as follows. Section 2 briefly describes the OGCM, observational data, and methodology used in this study. Section 3 provides the results of OGCM including variability of the NPSTMW volume and its budget analysis. Sections 4 and 5 present a cause of the epoch-dependent changes in driving mechanism for the NPSTMW formation. Section 6 summarizes and discusses this study.

2. Data and Methods

2.1. Model Description

The global OGCM used in this study is based on the Modular Ocean Model version 4.1 of Geophysical Fluid Dynamics Laboratory. The OGCM solves the primitive equations under Boussinesq and hydrostatic approximation with Arakawa-B grid system (Arakawa & Lamb, 1977). The OGCM has an eddy-permitting grid resolution of 1/4° in both longitudinal and latitudinal directions and 50 vertical levels of z^* vertical coordinate (Adcroft & Campin, 2004) with enhanced resolution near the surface. For better representation of the bottom topography, the partial step method (Adcroft et al., 1997; Pacanowski & Gnanadesikan, 1998) is employed to the thickness of bottom cell. A tri-polar grid system (Murray, 1996) is adopted with three poles located at Canada (100°W, 65°N), Russia (80°E, 65°N), and Antarctica to avoid the spherical coordinate singularity at the North Pole. The model topography is derived from the Ocean Circulation and Climate

Advanced Modelling project 1/10° bathymetric data set from the Southampton Oceanography Centre. For the vertical mixing, we used the K-profile parameterization (Large et al., 1994). The effect of tidal mixing is parameterized by following the methods of Simmons et al. (2004) and Lee et al. (2006), respectively. Horizontal viscosity is determined by the Smagorinsky biharmonic scheme (Griffies & Hallberg, 2000) without explicit lateral diffusion. The multidimensional, piecewise method scheme (Colella & Woodward, 1984) and a second-order centered finite difference scheme are applied to calculate the tracer and momentum advection, respectively. Other details of numerical methods in this experiment are based on the oceanic configuration of CM2.5 (Delworth et al., 2012).

The initial condition of the OGCM is set with January-February-March mean temperature and salinity derived from the World Ocean Atlas 2009 (Antonov et al., 2010; Locarnini et al., 2010). The OGCM is spun up over 50 years under the surface heat, freshwater, and momentum fluxes estimated by bulk formula (Large & Yeager, 2004) with the climatological variables of the Coordinated Ocean-sea ice Referenced Experiments phase 2 (CORE2)-Normal Year Forcing data set (Large & Yeager, 2009). After the spin-up, the hindcast model is integrated for 61 years from 1949 to 2009 with the annually varying CORE2-Inter-Annual Forcing data set (Large & Yeager, 2009). The sea surface salinity is restored to the climatological monthly mean salinity of Polar Hydrographic Climatology (Steele et al., 2001) with a damping timescale of 60 days. It takes about 11 years to reach a stationary equilibrium state for the eddy kinetic energy of upper 400 m in the western North Pacific region. Because the NPSTMW is mainly located in the upper 400 m, last 50 years (1960–2009) will be sufficient to investigate the interannual to decadal variability of the NPSTMW. We considered the main formation area of the NPSTMW near the KE (135–164°E and 30–42°N; box in Figures 1b and 1d) as a study region. The domain defined here is a few degrees north of that in the observations (Cerovečki & Giglio, 2016: 20–40°N; Qiu & Chen, 2006: 31–38°N) due to the overshooting of the Kuroshio in the OGCM which will be shown in section 2.4.

2.2. NPSTMW Definition and Volume Budget Analysis

We defined the NPSTMW with a potential density anomaly (σ_θ) range of 25.1–25.7 kg m^{-3} and the low PV ($<1.5\times10^{-10}$ m^{-1} s^{-1}) conditions. The PV is defined as

$$\mathrm{PV}=-\frac{f}{\rho_0}\frac{\partial\rho}{\partial z}, \tag{1}$$

where f is the Coriolis parameter. ρ_0 and ρ are the mean (1,025 kg m^{-3}) and anomalous potential density of seawater, respectively. We followed Uehara et al.'s (2003) threshold of the low PV, who adopted a stricter PV criterion (PV $< 1.5\times10^{-10}$ m^{-1} s^{-1}), smaller than the typical value (PV $< 2.0\times10^{-10}$ m^{-1} s^{-1}) applied to observation. The stricter PV criterion constrains the modelled NPSTMW volume to be consistent with the observation using typical threshold (Figure 2). Additionally, the minimum thickness of the NPSTMW was set to 50 m as suggested by Douglass et al. (2012). The volume of NPSTMW is calculated by multiplying the thickness (h) of NPSTMW by the grid size ($dx\times dy$) in each grid cell. In this study, the interannual variations of the volume of the NPSTMW are represented by its time series in March, when the maximum volume of the NPSTMW usually appears (Rainville et al., 2014; Suga & Hanawa, 1990).

To quantitatively analyze how the NPSTMW is formed during cooling seasons, the volume budget analysis is conducted using Walin framework (Cerovečki & Giglio, 2016; Guo et al., 2018; Rainville et al., 2007; Walin, 1982). Following Guo et al. (2018), the conservation equation for a control volume (V) bounded by σ_1 and σ_2 isopycnals can be obtained as

$$\frac{\partial V}{\partial t}=\int_{\sigma_1}^{\sigma_2}\left[-\frac{\partial}{\partial\sigma}\iint_{outcrop}-\frac{\alpha Q}{c_p}+\beta\rho S(E-P)dA_{surf}\right]d\sigma-\iint_{outcrop}\left(-\frac{\partial h}{\partial t}-U_h\cdot\nabla h-w_h\right)dA_{ml}-\iint\boldsymbol{u}\cdot\boldsymbol{n}dA_{lateral}, \tag{2}$$

where α and β are the thermal expansion and saline contraction coefficients, c_p is the specific heat, Q is the net surface heat flux (negative/positive for ocean heat loss/gain), ρ is the sea surface density, S is the sea surface salinity, E and P are the evaporation and precipitation, respectively, A_{surf} is the surface density outcrop area between σ_1 and σ_2 isopycnals; h is the MLD ($\Delta\sigma_\theta=0.03$ kg m^{-3}), U_h is lateral velocity integrated from the surface to base of mixed layer, w_h is vertical velocity at the base of mixed layer, and A_{ml} is density outcrop area ($\sigma_1\le\sigma<\sigma_2$) at the base of mixed layer; $\boldsymbol{u}$ is horizontal velocity, $\boldsymbol{n}$ is normal unit vector of the lateral boundary

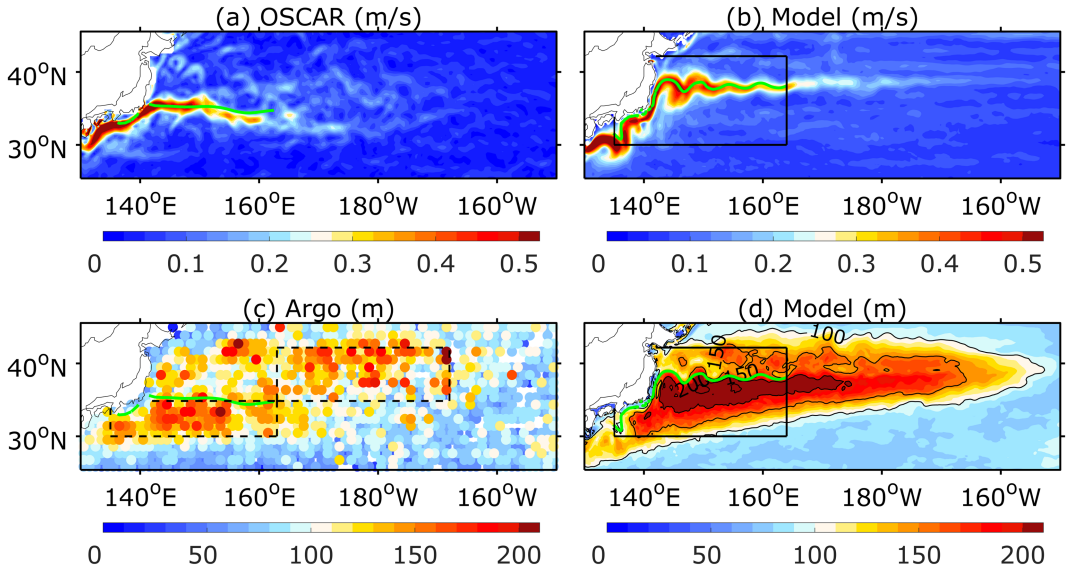

Figure 1. Climatological mean sea surface current speed (m s^{-1}) for (a) the observation (OSCAR, 1998–2011) and (b) the OGCM (1998–2009) during the cooling seasons (December to following March). Mixed layer depth (m, $\Delta\sigma_\theta = 0.03$ kg m^{-3}) from (c) the Argo observation (2000–2013, Holte et al., 2017) and (d) the OGCM (2000–2009) during the cooling seasons. Green lines indicate the Kuroshio main axis defined as the 12 °C isotherm at the depth of 300 m from (a,c) the World Ocean Atlas 2009 and (b,d) the OGCM. Dashed-line boxes in (c) indicate the formation area of the North Pacific subtropical mode water and central mode water (Kobashi et al., 2006; Oka & Qiu, 2012). Box in (b) and (d) indicates the study region in this study.

(outward positive), and $A_{lateral}$ is the element of area between σ_1 and σ_2 isopycnals at the lateral surface of four (east, west, south, and north) lateral open boundaries in the analysis domain. The left-hand side of equation (2) is the temporal changes of the control volume; the first, second, and third terms of the right-hand side of equation (2) represent surface transformation rate, vertical entrainment/detrainment rate, and advective volume flux through the lateral boundary in a control domain, respectively. We note that the second term is estimated in the mixed layer for the NPSTMW properties. In the KE region, the surface transformation rate term is mainly determined by the thermal (Q) forcing rather than the haline (E–P) forcing (Rainville et al., 2007). The vertical entrainment/detrainment rate term is mainly controlled by the temporal change of the MLD ($\partial h/\partial t$) in the KE region (Xu et al., 2014). The isopycnal surface σ_1 and σ_2 are set to 25.1 and 25.7 kg m^{-3}, respectively, which are lower and upper boundary of NPSTMW density range.

In order to focus on the formation process of the NPSTMW, equation (2) is integrated over the entire cooling season (December to following March; DJFM), when $\partial V/\partial t$ is positive (i.e., when the control volume increases),

$$\int_{DJFM} \frac{\partial V}{\partial t} dt = ASI + ENT + ADV + Residual, \quad (3)$$

where the left-hand side of equation (3) represents the amount of the volume formation in each cooling season. The terms named as ASI, ENT, and ADV in equation (3) represent the volume formed by the air-sea interaction, vertical entrainment, and advective flux, which can be obtained by time integrating the first, second, and third terms on the right-hand side of equation (2), respectively. The diapycnal diffusive flux is not considered here explicitly; thus, it is regarded as the residual term together with other imbalances including the volume difference between the bottom of mixed layer and the σ_2 density surface.

2.3. Statistical Methods and Supporting Observational Data

The statistical significance of the linear regression and the correlation coefficient is estimated by the block bootstrap method (Von Storch & Zwiers, 1999) with 1,000 resamples in blocks of three successive years to reflect the interannual persistence. The 21-year moving correlation analysis is conducted to examine the

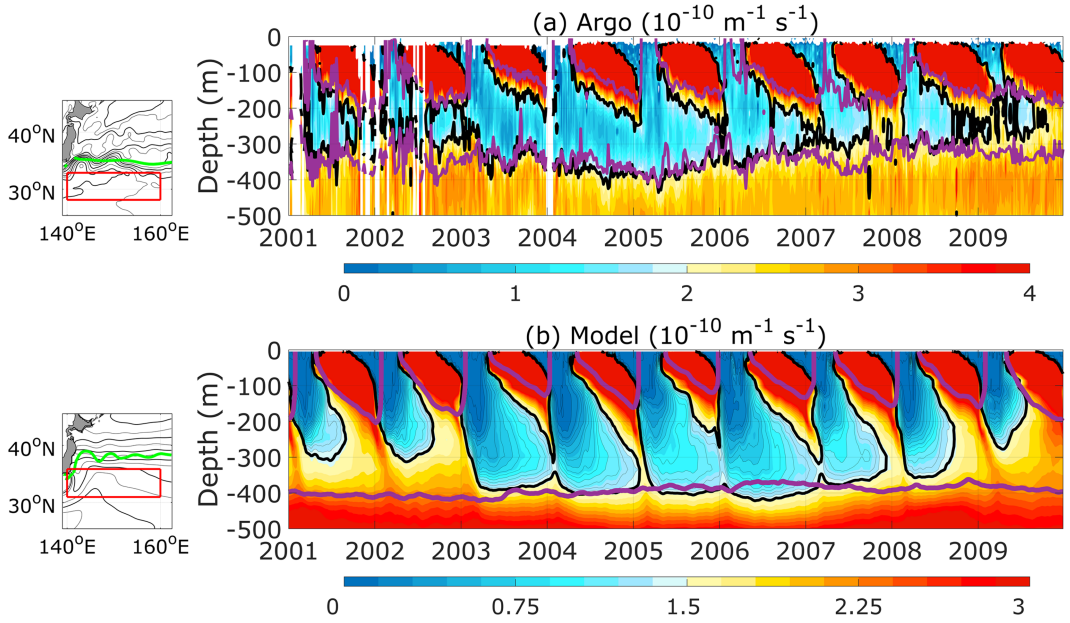

Figure 2. The depth-time sections of the domain average potential vorticity (PV) from five-daily mean data from (a) the Argo floats and (b) the OGCM. The analysis domains are 140–160°E, 28–33°N for the observation and 140–160°E, 31–36°N for the OGCM (red boxes in the thumbnail maps). Thick black contours indicate PV = 2.0×10^{-10} m^{-1} s^{-1} for the observation and PV = 1.5×10^{-10} m^{-1} s^{-1} for the OGCM. Solid purple lines indicate the isopycnal layers of σ_θ = 25.0, 25.5 kg m^{-3} for the observation and σ_θ = 25.1, 25.7 kg m^{-3} for the OGCM. Blanks in (a) indicate that the Argo data do not exist over 5 days in the analysis area. In the thumbnail maps, time mean sea surface height is contoured every 10 cm from the AVISO observation and the OGCM during the corresponding years. Green lines in the thumbnail maps indicate the 12 °C isotherm at the depth of 300 m representing the Kuroshio main axis from the World Ocean Atlas 2009 and the OGCM.

decadal changes of the interannual relationship between the NPSTMW volume and volume budget terms. The bootstrap method is also applied for each 21-year segment to determine the statistical significance of the moving correlation.

To quantify the interannual variability of the atmospheric forcing, we analyzed the two leading empirical orthogonal functions of the DJFM mean sea level pressure (SLP) anomaly from the CORE2-Inter-Annual Forcing in the North Pacific (120°E–120°W, 20–60°N) during 1960–2009. The first and second loading vectors of the SLP resemble the Aleutian Low mode pattern (Trenberth & Hurrell, 1994) and the North Pacific Oscillation (NPO) pattern (Linkin & Nigam, 2008), respectively. The second PC (PC-2) is considered as the NPO index (Yeh et al., 2018).

The performance of the OGCM is validated with the observation-based data sets. The surface current speed is validated with the near-surface current data obtained from Ocean Surface Current Analysis Real-time (OSCAR), derived from the various atmospheric and oceanic observations with 1/3° horizontal resolution from 1998 to 2011. The simulated sea surface height is compared to the 1/4° delayed mode daily absolute dynamic topography distributed by the Archiving, Validation, and Interpretation of Satellite Oceanographic data (AVISO). The simulated PV and the NPSTMW volume is validated with the EN4 data set (Good et al., 2013). We also use MLD interpolated in 1° grids (Holte et al., 2017) for 2000–2013 and Argo-derived subsurface PV values provided by Kuroshio Extension System Study (Rainville et al., 2014). The MLD is defined by the criterion with the density difference from the depth of 10 m as $\Delta\sigma_\theta = 0.03$ kg m^{-3}.

2.4. Model Validation

The OGCM reproduces strong surface currents along the Kuroshio path and major features of the KE such as the realistic quasi-stationary meanders (Figures 1a and 1b). However, compared with the OSCAR, there is an overshooting of the Kuroshio, which is a common feature in the eddy-resolving OGCM simulation (Masumoto et al., 2004) and even in the non-eddy-resolving OGCM simulation (Xu et al., 2014). In the observation, there are two separated regions showing deep MLD (>150 m) located south of Kuroshio (140–160°E,

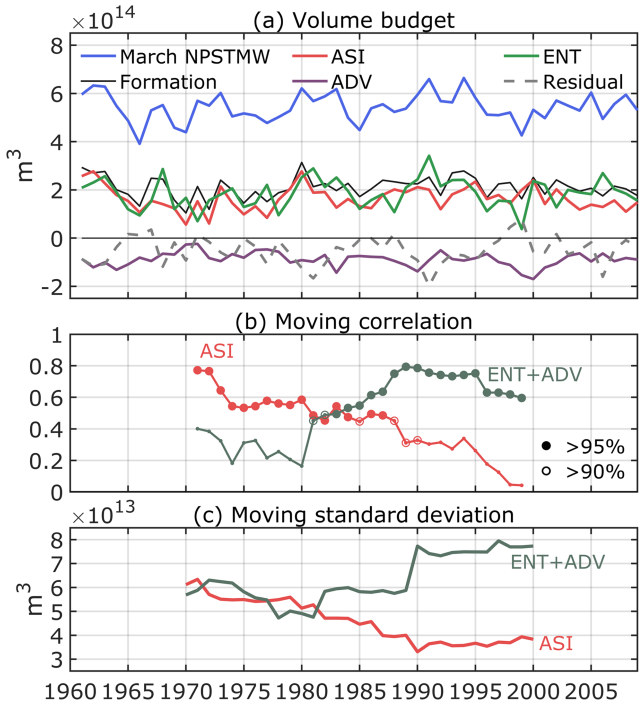

Figure 3. (a) Time series of volume of the NPSTMW in March (blue) and volume budget terms of equation (3). Volume budget terms integrated during cooling seasons (DJFM) include volume formation (black), air-sea interaction (ASI, red), advection (ADV, purple), vertical entrainment (ENT, green), and residual (dashed gray) terms. (b) The 21-year moving correlation coefficient of the NPSTMW volume in March with the air-sea interaction (red) and the ocean dynamics (vertical entrainment and advection, cobalt green) terms. Closed and open circles indicate significant correlation coefficients at the 95% and 90% confidence level, respectively. The 21-year moving correlation is the correlation between two time series within the window of ±10 years relative to the corresponding year. (c) The 21-year moving standard deviation of the air-sea interaction (red) and the ocean dynamics (cobalt green) terms.

30–35°N) and downstream region of Oyashio Extension (160°E–180°, 35–42°N) (Figure 1c). The OGCM well reproduces those deep MLD regions, although the separation into the two regions is not such clear (Figure 1d). This is also believed to be a common limitation of eddy-permitting OGCM simulations (Toyoda et al., 2004; Tsujino & Yasuda, 2004).

To validate the simulated NPSTMW in the formation area, we compare the domain-averaged PV of the OGCM with that in the Argo observation during the period of 2001–2009 (Figure 2). The low PV water is formed when the mixed layer gets deep during cooling season (December–March) in both the simulation and observation. It is trapped below the seasonal thermocline during the warming season (April–August) and finally reemerged to the sea surface in the following December, which is so-called the reemergence process of the NPSTMW (Alexander et al., 1999; Sugimoto & Hanawa, 2005). Although there is an overshooting of the Kuroshio, the interannual evolutions of the low PV water in the OGCM and the Argo observation are very similar (Figure 2). Therefore, we use the long-term OGCM result for investigating the formation mechanism of the NPSTMW over the longer period, in which the Argo data do not exist. We also compared the simulated interannual variation of the NPSTMW volume with that of the EN4 (Good et al., 2013) for the period of 1960–2009 and found a similar variation between the two ($r = 0.6$, not shown).

3. NPSTMW Formation and Its Variability

To quantitatively analyze how the NPSTMW is formed during winter, we estimated the volume budgets with equation (3) in the formation area of the NPSTMW. It is notable that the ASI (1.65×10^{14} m^3) and the ENT (1.85×10^{14} m^3) terms dominate the formation of the density class for the NPSTMW during 1961–2009 (2.11×10^{14} m^3) (Figure 3a). On the other hand, the ADV (-0.88×10^{14} m^3), which is dominated by the advection through the eastern boundary of the domain, shows a minor loss with limited variability. Also, the residual (-0.51×10^{14} m^3) term acts to lose the volume of the NPSTMW. This result is consistent with the findings by Rainville et al. (2007) and Cerovečki and Giglio (2016) based on observations. To investigate the contribution of the atmospheric and oceanic forcing on the NPSTMW formation, we divide the formation terms in equation (3) into two: local ASI and ocean dynamics. Here, ocean dynamics terms contain ENT and ADV terms in equation (3). Considering the mixed layer heat budget analysis, the ENT can be related with the ASI, because the ENT is also affected by the surface heat flux. However, we note that the ENT reflects primarily the ocean dynamics as its correlation with the ASI term is limited ($r = 0.27$) in the NPSTMW volume budget analysis. Furthermore, we note that the ENT term is more dominant over the ADV term in terms of the interannual variability of the ocean dynamics term (Figure 3a).

Strong interannual variability is observed in the time series of the volume budget terms, especially in the NPSTMW volume in March (blue line in Figure 3a) and DJFM integrated formation ($\partial V/\partial t$) term (black line in Figure 3a). Both time series show a similar temporal evolution during 1960–2009. Although the volume budget terms are calculated without imposing the low PV constraint, the annual formation amount of the NPSTMW density class in the volume budget is highly correlated with the NPSTMW volume in March, which is estimated with the PV constraint ($r = 0.71$). This result indicates that the non-PV volume budget terms in equation (3) can be used to assess how much each term contributes to the interannual variability of the NPSTMW volume in March. Therefore, we use the other budget terms (right-hand side of equation (3)) along with the NPSTMW volume in March to explain the contribution of the ASI and the ocean dynamics to the interannual variability of the NPSTMW volume.

To look into the change of driving factors for the NPSTMW formation, we calculate 21-year moving correlation coefficients between the NPSTMW volume and formation terms in equation (3) (Figure 3b). It is notable that there is a sudden change of the driving mechanism for the interannual variability of the NPSTMW volume around late-1980s. Before the period around late-1980s, the local ASI term is significantly correlated with the NPSTMW volume in March at 95% confidence level, while ocean dynamics terms have no significant correlation with it before early-1980s. Since late-1980s, the ocean dynamics exhibits a significant correlation with the NPSTMW volume at 95% confidence level, but the local ASI term does not. This is supported by the 21-year moving standard deviations of volume budget terms (Figure 3c) showing the increase (decrease) of the variability of the ocean dynamics (ASI) term after the late-1980s. The results are robust regardless of the moving window length between 19 and 23 years. The decadal change of the formation mechanism of the NPSTMW is also consistent with previous studies showing the winter regime shift of upper-layer thermal states around KE region (Pak et al., 2014, 2019; Park et al., 2012; Sugimoto & Kako, 2016). Considering the contrasts of the two moving correlation coefficients in Figure 3b, we separate the total analysis period into two distinct 21-year epochs, 1962–1982 and 1988–2008.

4. Relationship Between the NPSTMW and the Basin-Scale Atmospheric Variability

The dynamical and thermodynamical processes in the KE region are greatly affected by the local and lagged remote influences of the basin-scale climate variability (Kwon et al., 2010). Therefore, large-scale climate variability in the North Pacific can be a key to explain the interannual variability of the NPSTMW formation. Comparing the March NPSTMW volume time series with the leading PC times series of basin-scale SLP, we find significant relationship between the NPSTMW volume in March and the NPO index during the whole analysis period (Figure 4a). The NPO has marginally significant correlation with the NPSTMW volume ($r = -0.29$), and the correlation coefficient between the PC-1 and the NPSTMW volume is insignificant ($r = 0.11$). More importantly, the lag correlations between the NPO index and the NPSTMW volume in March show that the NPO exhibits a statistically significant correlation with the NPSTMW volume at different time lags in the two periods (Figures 4b and 4c).

During the period of 1962–1982, the NPO index is concurrently correlated with the volume of the NPSTMW in March (Figure 4b; $r = -0.46$). Note that there is no significant correlation, when the NPO index leads the NPSTMW volume. It implies that the interannual variability of the formation of the NPSTMW is related to the simultaneous atmospheric forcing associated with NPO in this period. This is consistent with Pak et al. (2014) who showed that the winter SST variability in the western North Pacific is under the influence of the mutually correlated EAWM and NPO patterns before the 1987/1988 regime shift. Due to the interannual variability of the atmospheric condition is strong in the western North Pacific during the former period (Pak et al., 2014, 2019), the NPSTMW volume variability is likely dominated by local air-sea interaction. This is consistent with the volume budget analysis showing the stronger variability of the ASI term during the former period (Figure 3c).

During the period of 1988–2008, the correlation coefficient between the NPO index and the NPSTMW volume in March is maximum ($r = 0.51$), when the NPO leads by 4 years (Figure 4c). The 4-year lag is consistent with the first mode baroclinic Rossby wave propagation timescale from the central North Pacific to reach the KE region (Qiu & Chen, 2010; Sugimoto & Hanawa, 2010), where the NPSTMW is mainly formed. Sugimoto and Hanawa (2010) reported that the Aleutian Low activity related to the West Pacific teleconnection pattern (Barnston & Livezey, 1987; Wallace & Gutzler, 1981), upper-level expression of the NPO, influences the formation of the NPSTMW by affecting the main thermocline depth variations in the central North Pacific via the westward Rossby wave propagation. When the NPO is positive, the deeper thermocline propagated from the central North Pacific can be a precondition for the deeper MLD in the formation area of the NPSTMW and, in turn, increase the NPSTMW formation. On the other hand, the simultaneous correlation coefficient between the NPO and the NPSTMW volume gets insignificant, suggesting that the local atmospheric forcing associated with NPO has minor influence on the NPSTMW variability (Figure 4c).

The Hovmöller diagram for the anomalies of DJFM $\sigma_\theta = 25.7$ kg m^{-3} (here after 25.7 σ_θ) isopycnal surface depth, which corresponds to the lower boundary of the NPSTMW, between 33°N and 37°N supports the

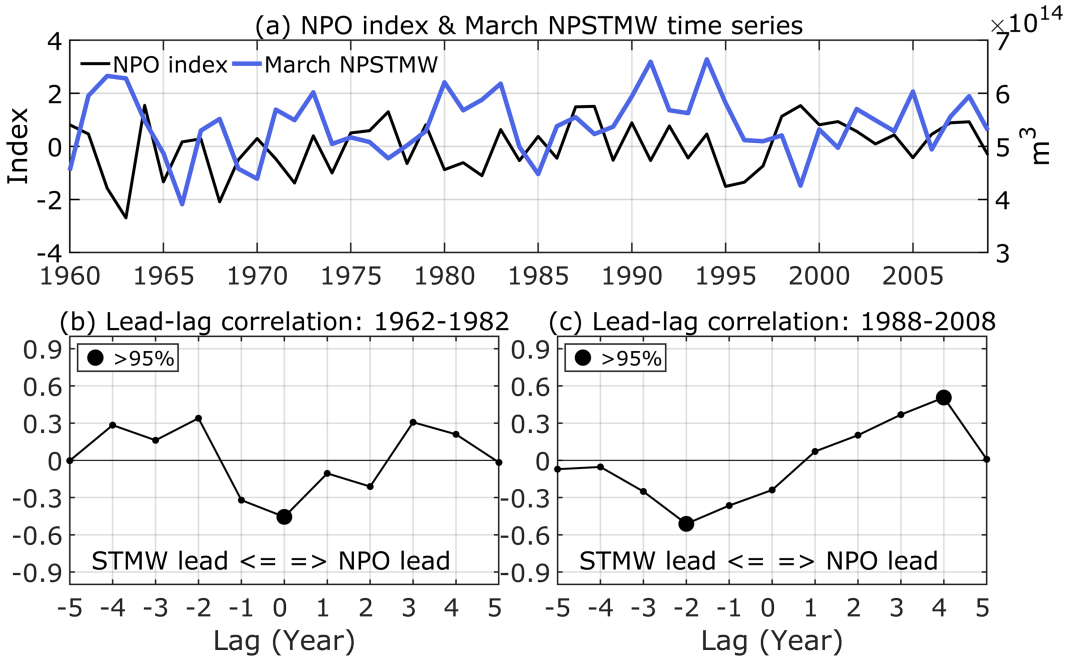

Figure 4. (a) Time series of the NPO index (empirical orthogonal function PC-2 of sea level pressure anomaly) (black) and the NPSTMW volume in March (blue). (b,c) Lead-lag correlation between the NPO index and the NPSTMW volume in March during (b) 1962–1982 and (c) 1988–2008. Positive lag indicates that NPO index leads the NPSTMW volume. Black circle indicates significant values at the 95% confidence level.

presence of the westward wave propagation during the later period (Figure 5a). Although the isopycnal of 25.7 σ_θ does not include the PV criterion, its temporal evolution is quite similar with that of the vertically averaged PV anomaly in the NPSTMW isopycnal layer as reported by Cerovečki and Giglio (2016) (see their figures 15 and 16). We choose the latitude band 33–37°N to consider the model bias due to the Kuroshio overshooting. Even if the target domain is shifted by several degrees in the latitudinal direction compared to the observational analyses by Cerovečki and Giglio (2016), the results are comparable. After 1990, the Hovmöller diagram shows the westward propagation signal of the anomalies of 25.7 σ_θ isopycnal surface depth over 3–4 years from the central North Pacific. The zonally averaged 25.7 σ_θ isopycnal depth between 160°E and 180° exhibits significant maximum correlation with that between 140°E and 145°E when the former leads by 4 years during 1988–2008 (r = 0.45) (Figure 5b). This lag correlation suggests a delayed response of the NPSTMW volume to the anomalies of 25.7 σ_θ isopycnal depth in the central North Pacific. The westward propagating speed is about 3.2 cm s^{-1}, which is very similar to that estimated by Qiu and Chen (2010) (3.7 cm s^{-1}) in the latitude 32–34°N band based on the satellite altimeter. On the contrary, during the former period, the westward propagation is not clear ($r = -0.28$) (Figures 5a and 5b).

Note that there is a hint of ocean-to-atmospheric feedback when NPSTMW leads NPO by 2 years during 1988–2008 (Figure 4c), which is consistent with Ceballos et al. (2009, see their figure 3b), who mentioned the self-sustained oscillation between the ocean and atmosphere. However, we here focus only on the response of the NPSTMW to the climate variability.

We also calculate the correlation coefficients between the SLP PC-1 and the volume of the NPSTMW in March. While the correlation is not statistically significant for the entire period or the early period (1962–1982), it becomes significant ($r = -0.52$) during the period of 1988–2008 when the SLP PC-1 leads by 1 year. This result may be consistent with that of Na et al. (2018), who showed that the variability of the meridional movement of the KE-subarctic frontal zone is strongly correlated by 1-year lag to the Pacific Decadal Oscillation, while the variability of the KE strength is related to the North Pacific Gyre Oscillation by 4-year lag. The fast response by 1 year of the NPSTMW volume may be associated with a barotropic response to the Pacific-North American teleconnection pattern-like variability.

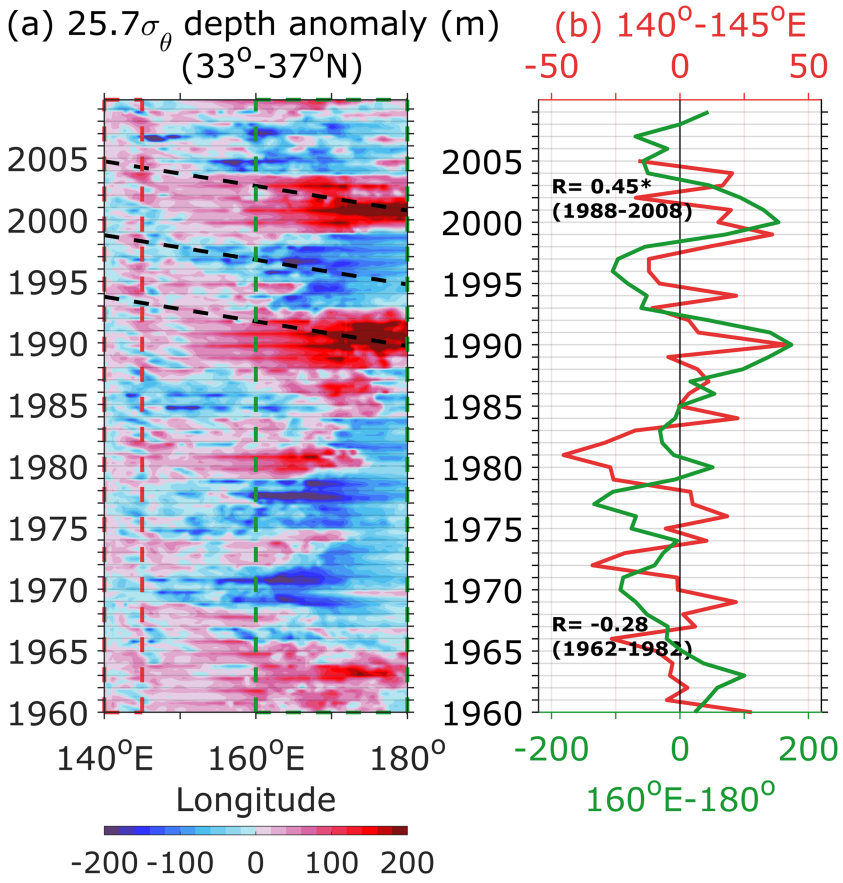

Figure 5. (a) The time-longitude Hovmöller diagram of DJFM $\sigma_\theta = 25.7$ kg m^{-3} isopycnal surface depth anomaly, which is meridionally averaged between 33°N and 37°N during 1960–2009. The thick dashed line indicates the westward propagating $\sigma_\theta = 25.7$ kg m^{-3} isopycnal surface depth anomaly. (b) Comparison between DJFM mean depth anomaly of $\sigma_\theta = 25.7$ kg m^{-3} isopycnal surface averaged in central North Pacific region (160°E–180°, 33–37°N, green) and that of western North Pacific region (140–145°E, 33–37°N, red). The time axis of western North Pacific region (black line) is shifted −4 years to highlight the lagged relationship between two time series. Asterisk mark indicates statistically significant at the 90% confidence level.

5. Possible Reasons for the Regime Shift in the Driving Mechanism of the NPSTMW Formation

According to the preceding section, one of the key differences between the two contrasting epochs is the presence of the Rossby wave propagation from the central North Pacific to the NPSTMW region. First of all, the epoch-dependent presence of the Rossby wave propagation can be attributed to the suppression due to the strong local atmospheric variability. In addition, the remote forcing may have been much weaker (stronger) to begin with during the former (later) period. The zonal distribution of the wind stress curl (WSC) is examined to investigate the local and remote WSC forcing in two contrasting periods. Figure 6a shows the Hovmöller diagram of the DJFM WSC (estimated from the input wind fields) meridionally averaged between 33°N and 37°N, which corresponds to the main formation area of the NPSTMW. The most noticeable difference between the two epochs is the zonal location of the largest WSC anomalies. Prior to the late-1980s, the WSCs are overall zonally uniform over 140°E–180°, and the largest positive anomalies are found in the NPSTMW formation region (145–155°E). On the other hand, after late-1980s, the sign of the large WSC around the dateline is generally opposite to the weaker anomalies near the formation area of the NPSTMW (140–160°E).

More importantly, the thermocline anomalies produced by the large WSC anomalies in the central North Pacific 4 years prior are not opposed by the large positive WSC anomalies in the NPSTMW formation

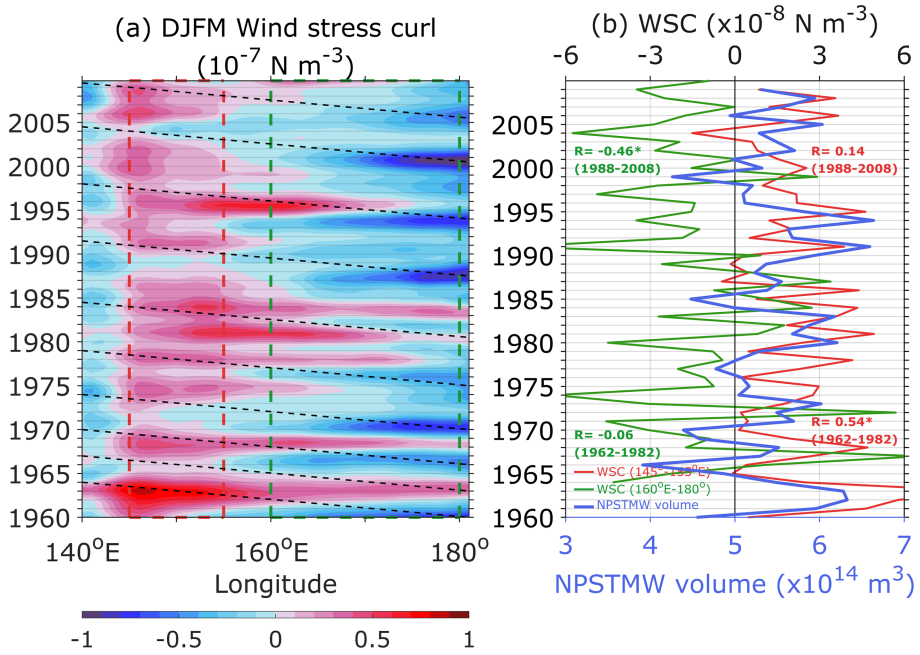

Figure 6. (a) The time-longitude Hovmöller diagram of the 3-year low-pass filtered DJFM wind stress curl, which is meridionally averaged between 33°N and 37°N. (b) Comparison between the NPSTMW volume in March (blue line) and the wind stress curl averaged in the NPSTMW formation region (145–155°E, 33–37°N, red line) and central North Pacific region (160°E–180°, 33–37°N, green line). The time axis of central North Pacific region (green line) is shifted +4 years to highlight the lagged relationship with the NPSTMW volume in March (blue line). Asterisk mark indicates statistically significant at the 90% confidence level.

region, as they propagate westward via Rossby wave, since late-1980s. Therefore, the large remote WSC anomalies can effectively influence the formation of the NPSTMW (Qiu et al., 2014). Conversely, the effect of weaker remote WSC anomalies on the thermocline during the early period is often opposed by larger local WSC anomalies in the NPSTMW formation region; thus, the zonally uniform WSC distribution during the former period is not favorable to produce the propagating Rossby waves (Figure 6a).

The epoch-dependent role of the remote and local WSC distributions is further supported by their respective correlation with the NPSTMW volume (Figure 6b). The zonal averages of the WSC between 145°E and 155°E show significant simultaneous correlation with the NPSTMW volume in March during 1962–1982 ($r = 0.54$), while the impact of the local WSC on the NPSTMW is not significant during 1988–2008 ($r = 0.14$; Figure 6b). On the other hand, the zonal averages of the WSC between 160°E and 180° show significant 4-year leading correlation with the NPSTMW volume in March during 1988–2008 ($r = -0.46$; Figure 6b), suggesting the delayed response of the NPSTMW volume to the WSC in the central North Pacific. Also, the corresponding 4-year lag correlation during the former period is insignificant ($r = -0.06$).

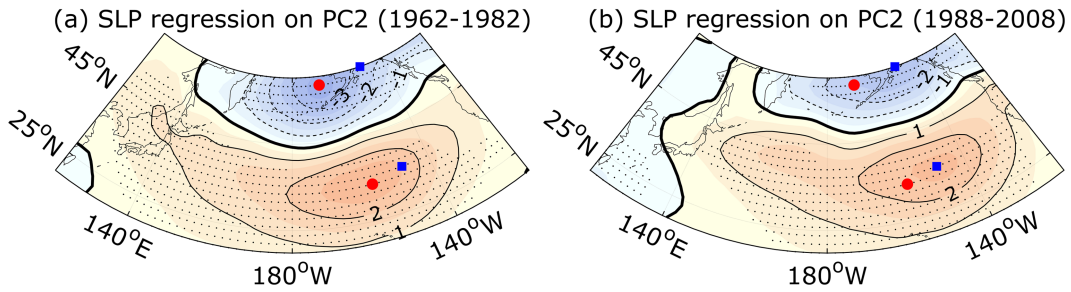

Figure 7. Regression maps of anomalous winter (DJF) sea level pressure on the NPO index for the period of (a) 1962–1982 and (b) 1988–2008. Red dots and blue squares represent the two centers of action of NPO during 1962–1982 and 1988–2008, respectively. Black dots indicate regions where the regression coefficients are statistically significant at the 90% confidence level.

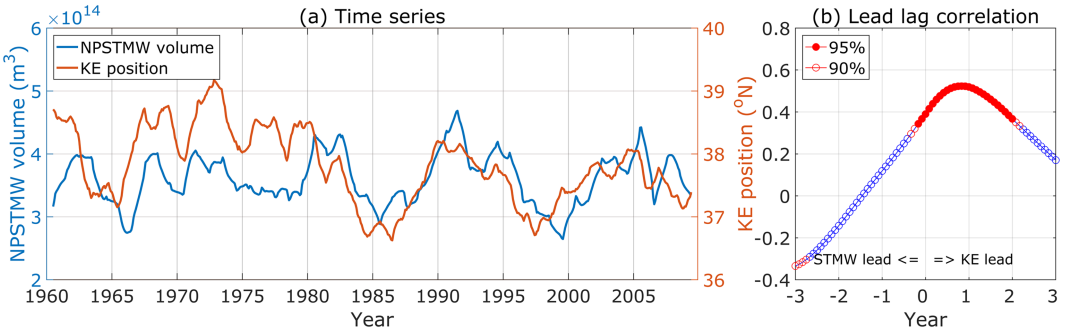

Figure 8. (a) Time series of the 12-month moving averaged NPSTMW volume (blue) and the latitudinal position of the Kuroshio main axis zonally averaged from 141°E to 158°E (red). Kuroshio main axis is defined by the 40-cm contour of the sea surface height. (b) Lead-lag correlation between the latitudinal position of the Kuroshio main axis and the NPSTMW volume. Positive lag indicates that the latitudinal position of the Kuroshio main axis leads the NPSTMW volume. Closed and open red circles indicate significant values at the 95% and 90% confidence level, respectively.

Although the cause of the change in the WSC may be arguable and beyond the scope of this study, it is consistent with the eastward movement of the NPO center after mid-1990s (Yeh et al., 2018). Figure 7 shows the regressed SLP on the NPO index of each period. During 1962–1982, the dipole centers are located on 157°W with strong north-south SLP gradient. It appears that the center moves eastward by 10° and the SLP gradient is decreased at the same time during 1988–2008. Pak et al. (2014) also showed that the EAWM and NPO were significantly correlated to each other during the 1973–1987 strong winter monsoon epoch, but their correlation practically vanishes during the 1988–2002. They also reported that the EAWM's impact on SST during the latter epoch shrank remarkably into a limited area in the East China Sea, making a clear distinction from the NPO impact. Therefore, we suppose that the eastward shift of the NPO causes the change in the zonal distribution of WSC. When the NPO centers are placed closer to the KE region before the late-1980s, the direct local atmospheric forcing associated with the NPO dominantly influences the formation of the NPSTMW and suppresses the effect of the remote forcing, while the former weakens and is replaced by the latter when the NPO moved eastward after the late-1980s.

6. Summary and Discussion

A 50-year (1960–2009) hindcast of the OGCM reproduces well the features of the NPSTMW formation during cooling seasons and its epoch-dependent variability. Based on the moving correlation analysis, we have shown that there is change in the main driving mechanism for the interannual variability of the NPSTMW volume in March around late-1980s. During 1962–1982, the local air-sea flux is primarily responsible for the most of the interannual variability of the NPSTMW volume, while it is mostly controlled by ocean dynamics associated with the westward propagating Rossby waves during 1988–2008. The NPSTMW volume has a statistically significant correlation with the NPO over the entire period, though the time lag is different in the two periods. In addition to the changes in the correlation, the changes in the relative amplitudes of the ocean dynamics and air-sea flux terms also contribute to this epoch-dependent formation mechanism of the NPSTMW. The change in the amplitude of variability in these terms is shown to be associated with the differences in the WSC during the two periods. During the earlier epoch, the strong local WSC in the western North Pacific primarily contributes to the formation of the NPSTMW and suppresses the effect of the remote oceanic forcing, while it has weakened and create favorable conditions for the westward Rossby wave propagation during the later epoch.

The findings in this study are in line with the previous studies showing the regime shift of the upper-ocean thermal states, such as the MLD (Sugimoto & Kako, 2016) and the SST (Pak et al., 2014, 2019; Park et al., 2012), occurred in late-1980s. However, these studies do not focus on the "NPSTMW water mass" itself. Although Sugimoto and Kako (2016) investigated nonstationary driving mechanism for the decadal changes of the winter MLD variability, the MLD alone cannot explain the formation mechanism of the NPSTMW, because the NPSTMW formation is affected by various oceanic and atmospheric processes as discussed in

section 2.2. In this study, we explicitly investigate the interannual variability of the NPSTMW formation using the volume budget analysis and find a regime shift of the driving mechanism for the NPSTMW formation in late-1980s.

During the warm season, the NPSTMW is subducted below the seasonal thermocline with the memories of the wintertime information; thus, it could affect year to year the basin-scale climate variability as shown in Figure 4c. Therefore, the interannual variability of the NPSTMW formation may be important for understanding the oceanic impact on the long-term climate variability. The importance of this study is that late-1980s regime shift in the formation mechanism is reported for the first time. In addition, this study provides robust complementary evidences to support the previous observational results by using a long-term eddy-permitting OGCM simulation.

Several previous studies suggested that the local ocean current (KE) instability also affects the variability of the low PV water volume in the KE region (Oka et al., 2019; Qiu & Chen, 2006; Xu et al., 2014). In this study, the relationship between the NPSTMW variability and the KE variability has not been specifically investigated, though the meridional movement of the KE axis is significantly correlated with the NPSTMW volume when the KE leads by 1 year ($r = 0.52$) (Figure 8). More importantly, the two are much better correlated in the later epoch, which implies that the KE change is a part of the increased ocean dynamic's contribution in the later epoch. Whether the instability of KE, which can change the local ocean stratification, specifically plays a role needs to be further investigated in the future. Further study is also needed to identify the effect of the ocean stratification on the NPSTMW formation. Besides that, there are several unsolved questions from this study. For example, possible mechanisms for the significant correlation between the basin-scale climate variability and the NPSTMW volume, when the latter leads the former by several years, are not yet clear. We suggest that long-term numerical simulation using the fully coupled atmosphere-ocean model will be useful to examine the potential ocean-to-atmosphere feedback.

Acknowledgments
The CORE2 data set was obtained from https://data1.gfdl.noaa.gov/nomads/forms/core/COREv2.html. The World Ocean Atlas 2009 and the Polar Hydrographic Climatology data set were obtained from https://www.nodc.noaa.gov/OC5/WOA09/pr_woa09.html and http://psc.apl.washington.edu/nonwp_projects/PHC/Climatology.html, respectively. The OSCAR data were taken from https://podaac.jpl.nasa.gov/dataset/OSCAR_L4_OC_third-deg. The database of mixed layer depth is downloaded from http://mixedlayer.ucsd.edu. The data set of the Argo floats was taken from http://uskess.whoi.edu/. The sea surface height data observed by the satellite are available from AVISO (http://www.aviso.altimetry.fr/duacs/). The EN4 data set was downloaded from https://www.metoffice.gov.uk/hadobs/en4/. This study was supported by the National Research Foundation of Korea (NRF) Grant NRF-2009-C1AAA001-0093, funded by the Korea government (MEST). The numerical simulation in this paper was supported by the Supercomputing Center of Korea Institute of Science and Technology Information (KISTI), with its supercomputing resources and technical support (KSC-2018-CRE-0117). Y.-O. Kwon was funded by National Science Foundation (NSF) EaSM2 OCE-1242989. Y. H. Kim was partly supported by research projects entitled “Investigation and prediction system development of marine heatwave around the Korean Peninsula originated from the subarctic and western Pacific” (20190344) funded by the Ministry of Oceans and Fisheries (MOF). G. Pak was supported by in-house projects of the Korea Institute of Ocean Science & Technology (PE99711, PE99811).

References

Adcroft, A., & Campin, J. M. (2004). Rescaled height coordinates for accurate representation of free-surface flows in ocean circulation models. *Ocean Modelling*, *7*(3-4), 269–284. https://doi.org/10.1016/j.ocemod.2003.09.003

Adcroft, A., Hill, C., & Marshall, J. (1997). Representation of topography by shaved cells in a height coordinate ocean model. *Monthly Weather Review*, *125*(9), 2293–2315. https://doi.org/10.1175/1520-0493(1997)125<2293:ROTBSC>2.0.CO;2

Alexander, M. A., Deser, C., & Timlin, M. S. (1999). The reemergence of SST anomalies in the North Pacific Ocean. *Journal of Climate*, *12*(8), 2419–2433. https://doi.org/10.1175/1520-0442(1999)012<2419:TROSAI>2.0.CO;2

Antonov, J. I., Seidov, D., Boyer, T. P., Locarnini, R. A., Mishonov, A. V., Garcia, H. E., et al. (2010). In S. Levitus (Ed.), *World Ocean Atlas 2009, vol. 2, Salinity*, NOAA Atlas NESDIS (Vol. *69*, p. 184). Silver Spring, MD: NOAA.

Arakawa, A., & Lamb, V. R. (1977). Computational design of the basic dynamical processes of the UCLA general circulation model. *Methods in Computational Physics: Advances in Research and Applications*, *17*, 173–265. https://doi.org/10.1016/B978-0-12-460817-7.50009-4

Barnston, A. G., & Livezey, R. E. (1987). Classification, seasonality and persistence of low-frequency atmospheric circulation patterns. *Monthly Weather Review*, *115*(6), 1083–1126. https://doi.org/10.1175/1520-0493(1987)115<1083:CSAPOL>2.0.CO;2

Bates, N. R. (2012). Multi-decadal uptake of carbon dioxide into subtropical mode water of the North Atlantic Ocean. *Biogeosciences*, *9*(7), 2649–2659. https://doi.org/10.5194/bg-9-2649-2012

Bingham, F. M. (1992). Formation and spreading of subtropical mode water in the North Pacific. *Journal of Geophysical Research*, *97*(C7), 11,177–11,189. https://doi.org/10.1029/92JC01001

Ceballos, L. I., Di Lorenzo, E., Hoyos, C. D., Schneider, N., & Taguchi, B. (2009). North Pacific gyre oscillation synchronizes climate fluctuations in the eastern and western boundary systems. *Journal of Climate*, *22*(19), 5163–5174. https://doi.org/10.1175/2009JCLI2848.1

Cerovečki, I., & Giglio, D. (2016). North Pacific subtropical mode water volume decrease in 2006–09 estimated from Argo observations: Influence of surface formation and basin-scale oceanic variability. *Journal of Climate*, *29*(6), 2177–2199. https://doi.org/10.1175/JCLI-D-15-0179.1

Colella, P., & Woodward, P. R. (1984). The piecewise parabolic method (PPM) for gas-dynamical simulations. *Journal of Computational Physics*, *54*(1), 174–201. https://doi.org/10.1016/0021-9991(84)90143-8

Delworth, T. L., Rosati, A., Anderson, W., Adcroft, A. J., Balaji, V., Benson, R., et al. (2012). Simulated climate and climate change in the GFDL CM2.5 high-resolution coupled climate model. *Journal of Climate*, *25*(8), 2755–2781. https://doi.org/10.1175/JCLI-D-11-00316.1

Douglass, E. M., Jayne, S. R., Peacock, S., Bryan, F. O., & Maltrud, M. E. (2012). Subtropical mode water variability in a climatologically forced model in the northwestern Pacific Ocean. *Journal of Physical Oceanography*, *42*(1), 126–140. https://doi.org/10.1175/2011JPO4513.1

Good, S. A., Martin, M. J., & Rayner, N. A. (2013). EN4: Quality controlled ocean temperature and salinity profiles and monthly objective analyses with uncertainty estimates. *Journal of Geophysical Research: Oceans*, *118*, 6704–6716. https://doi.org/10.1002/2013JC009067

Griffies, S. M., & Hallberg, R. W. (2000). Biharmonic friction with a Smagorinsky viscosity for use in large-scale eddy-permitting ocean models. *Monthly Weather Review*, *128*(8), 2935–2946. https://doi.org/10.1175/1520-0493(2000)128<2935:BFWASL>2.0.CO;2
Guo, Y., Lin, X., Wei, M., Liu, C., & Men, G. (2018). Decadal variability of North Pacific eastern subtropical mode water. *Journal of Geophysical Research: Oceans*, *123*, 6189–6206. https://doi.org/10.1029/2018JC013890
Hanawa, K. (1987). Interannual variations of the winter-time outcrop area of subtropical mode water in the western North Pacific ocean. *Atmosphere-Ocean*, *25*(4), 358–374. https://doi.org/10.1080/07055900.1987.9649280
Hanawa, K., & Hoshino, I. (1988). Temperature structure and mixed layer in the Kuroshio region over the Izu Ridge. *Journal of Marine Research*, *46*(4), 683–700. https://doi.org/10.1357/002224088785113397
Holte, J., Talley, L. D., Gilson, J., & Roemmich, D. (2017). An Argo mixed layer climatology and database. *Geophysical Research Letters*, *44*, 5618–5626. https://doi.org/10.1002/2017GL073426
Kobashi, F., Mitsudera, H., & Xie, S.-P. (2006). Three subtropical fronts in the North Pacific: Observational evidence for mode water-induced subsurface frontogenesis. *Journal of Geophysical Research*, *111*, C09033. https://doi.org/10.1029/2006JC003479
Kwon, Y.-O., Alexander, M. A., Bond, N. A., Frankignoul, C., Nakamura, H., Qiu, B., & Thompson, L. (2010). Role of the Gulf Stream and Kuroshio-Oyashio systems in large-scale atmosphere-ocean interaction: A review. *Journal of Climate*, *23*(12), 3249–3281. https://doi.org/10.1175/2010JCLI3343.1
Large, W. G., McWilliams, J. C., & Doney, S. C. (1994). Oceanic vertical mixing: A review and a model with a nonlocal boundary layer parameterization. *Reviews of Geophysics*, *32*(4), 363–403. https://doi.org/10.1029/94RG01872
Large, W. G., & Yeager, S. G. (2004). Diurnal to decadal global forcing for ocean and sea-ice models: The data sets and flux climatologies (NCAR Tech. Rep. TN-460 + STR, 105 pp.). National Center for Atmospheric Research, Colo.
Large, W. G., & Yeager, S. G. (2009). The global climatology of an interannually varying air-sea flux data set. *Climate Dynamics*, *33*(2–3), 341–364. https://doi.org/10.1007/s00382-008-0441-3
Lee, H.-C., Rosati, A., & Spelman, M. J. (2006). Barotropic tidal mixing effects in a coupled climate model: Oceanic conditions in the Northern Atlantic. *Ocean Modelling*, *11*(3–4), 464–477. https://doi.org/10.1016/j.ocemod.2005.03.003
Linkin, M. E., & Nigam, S. (2008). The North Pacific Oscillation-west Pacific teleconnection pattern: Mature-phase structure and winter impacts. *Journal of Climate*, *21*(9), 1979–1997. https://doi.org/10.1175/2007JCLI2048.1
Locarnini, R. A., Mishonov, A. V., Antonov, J. I., Boyer, T. P., Garcia, H. E., Baranova, O. K., et al. (2010). In S. Levitus (Ed.), *World Ocean Atlas 2009, vol. 1, Temperature*, NOAA Atlas NESDIS (Vol. *69*, p. 184). Silver Spring, MD: NOAA.
Masumoto, Y., Sasaki, H., Kagimoto, T., Komori, N., Ishida, A., Sasai, Y., et al. (2004). A fifty-year eddy-resolving simulation of the world ocean: Preliminary outcomes of OFES (OGCM for the Earth Simulator). *Journal of the Earth Simulator*, *1*, 35–56.
Masuzawa, J. (1969). Subtropical mode water. *Deep Sea Research and Oceanographic Abstracts*, *16*(5), 463–472. https://doi.org/10.1016/0011-7471(69)90034-5
Murray, R. J. (1996). Explicit generation of orthogonal grids for ocean models. *Journal of Computational Physics*, *126*(2), 251–273. https://doi.org/10.1006/jcph.1996.0136
Na, H., Kim, K.-Y., Minobe, S., & Sasaki, Y. N. (2018). Interannual to decadal variability of the upper-ocean heat content in the western North Pacific and its relationship to oceanic and atmospheric variability. *Journal of Climate*, *31*(13), 5107–5125. https://doi.org/10.1175/JCLI-D-17-0506.1
Oka, E., & Qiu, B. (2012). Progress of North Pacific mode water research in the past decade. *Journal of Oceanography*, *68*(1), 5–20. https://doi.org/10.1007/s10872-011-0032-5
Oka, E., Yamada, K., Sasano, D., Enyo, K., Nakano, T., & Ishii, M. (2019). Remotely forced decadal physical and biogeochemical variability of North Pacific subtropical mode water over the last 40 years. *Geophysical Research Letters*, *46*, 1555–1561. https://doi.org/10.1029/2018GL081330
Pacanowski, R. C., & Gnanadesikan, A. (1998). Transient response in a Z-level ocean model that resolves topography with partial cells. *Monthly Weather Review*, *126*(12), 3248–3270. https://doi.org/10.1175/1520-0493(1998)126<3248:TRIAZL>2.0.CO;2
Pak, G., Park, Y.-H., Vivier, F., Kwon, Y.-O., & Chang, K.-I. (2014). Regime-dependent nonstationary relationship between the East Asian winter monsoon and North Pacific Oscillation. *Journal of Climate*, *27*(21), 8185–8204. https://doi.org/10.1175/JCLI-D-13-00500.1
Pak, G., Yeh, S.-W., Nam, S., Park, Y.-H., & Kim, Y. H. (2019). Major driver leading to winter SST variability in the Kuroshio recirculation gyre region and its decadal changes: Refreshing versus spring-initiated reemergence processes. *Geophysical Research Letters*, *46*, 272–280. https://doi.org/10.1029/2018GL081232
Park, Y.-H., Yoon, J.-H., Youn, Y.-H., & Vivier, F. (2012). Recent warming in the western North Pacific in relation to rapid changes in the atmospheric circulation of the Siberian high and Aleutian low systems. *Journal of Climate*, *25*(10), 3476–3493. https://doi.org/10.1175/2011JCLI4142.1
Qiu, B., & Chen, S. (2006). Decadal variability in the formation of the North Pacific subtropical mode water: Oceanic versus atmospheric control. *Journal of Physical Oceanography*, *36*(7), 1365–1380. https://doi.org/10.1175/JPO2918.1
Qiu, B., & Chen, S. (2010). Eddy-mean flow interaction in the decadal modulating Kuroshio Extension system. *Deep Sea Research, Part II*, *57*(13–14), 1098–1110. https://doi.org/10.1016/j.dsr2.2008.11.036
Qiu, B., Chen, S., Schneider, N., & Taguchi, B. (2014). A coupled decadal prediction of the dynamic state of the Kuroshio Extension system. *Journal of Climate*, *27*(4), 1751–1764. https://doi.org/10.1175/JCLI-D-13-00318.1
Rainville, L., Jayne, S. R., & Cronin, M. F. (2014). Variations of the North Pacific subtropical mode water from direct observations. *Journal of Climate*, *27*(8), 2842–2860. https://doi.org/10.1175/JCLI-D-13-00227.1
Rainville, L., Jayne, S. R., McClean, J. L., & Maltrud, M. E. (2007). Formation of subtropical mode water in a high-resolution ocean simulation of the Kuroshio Extension region. *Ocean Modelling*, *17*(4), 338–356. https://doi.org/10.1016/j.ocemod.2007.03.002
Simmons, H. L., Jayne, S. R., Laurent, L. C. S., & Weaver, A. J. (2004). Tidally driven mixing in a numerical model of the ocean general circulation. *Ocean Modelling*, *6*(3–4), 245–263. https://doi.org/10.1016/S1463-5003(03)00011-8
Steele, M., Morley, R., & Ermold, W. (2001). PHC: A global ocean hydrography with a high-quality Arctic Ocean. *Journal of Climate*, *14*(9), 2079–2087. https://doi.org/10.1175/1520-0442(2001)014<2079:PAGOHW>2.0.CO;2
Suga, T., & Hanawa, K. (1990). The mixed-layer climatology in the northwestern part of the North Pacific subtropical gyre and the formation area of subtropical mode water. *Journal of Marine Research*, *48*(3), 543–566. https://doi.org/10.1357/002224090784984669
Sugimoto, S., & Hanawa, K. (2005). Remote reemergence areas of winter sea surface temperature anomalies in the North Pacific. *Geophysical Research Letters*, *32*, L01606. https://doi.org/10.1029/2004gl021410
Sugimoto, S., & Hanawa, K. (2010). Impact of Aleutian Low activity on the STMW formation in the Kuroshio recirculation gyre region. *Geophysical Research Letters*, *37*, L03606. https://doi.org/10.1029/2009GL041795

Sugimoto, S., & Kako, S. (2016). Decadal variation in winter mixed layer depth south of the Kuroshio Extension and its influence on winter mixed layer temperature. *Journal of Climate*, *29*(3), 1237–1252. https://doi.org/10.1175/JCLI-D-15-0206.1

Toyoda, T., Awaji, T., Ishikawa, Y., & Nakamura, T. (2004). Preconditioning of winter mixed layer in the formation of north Pacific eastern subtropical mode water. *Geophysical Research Letters*, *31*, L17206. https://doi.org/10.1029/2004GL020677

Trenberth, K. E., & Hurrell, J. W. (1994). Decadal atmosphere-ocean variations in the Pacific. *Climate Dynamics*, *9*(6), 303–319. https://doi.org/10.1007/BF00204745

Tsujino, H., & Yasuda, T. (2004). Formation and circulation of mode water of the north Pacific in a high-resolution GCM. *Journal of Physical Oceanography*, *34*(2), 399–415. https://doi.org/10.1175/1520-0485(2004)034<0399:FACOMW>2.0.CO;2

Uehara, H., Suga, T., Hanawa, K., & Shikama, N. (2003). A role of eddies in formation and transport of North Pacific subtropical mode water. *Geophysical Research Letters*, *30*(13), 1705. https://doi.org/10.1029/2003GL017542

Von Storch, H., & Zwiers, F. W. (1999). *Statistical analysis in climate research* (p. 494). Cambridge: Cambridge University Press.

Walin, G. (1982). On the relation between sea surface heat flow and thermal circulation in the ocean. *Tellus*, *34*(2), 187–195. https://doi.org/10.3402/tellusa.v34i2.10801

Wallace, J. M., & Gutzler, D. S. (1981). Teleconnections in the geopotential height field during the northern hemisphere winter. *Monthly Weather Review*, *109*(4), 784–812. https://doi.org/10.1175/1520-0493(1981)109<0784:TITGHF>2.0.CO;2

Xu, L., Xie, S.-P., McClean, J. L., Liu, Q., & Sasaki, H. (2014). Mesoscale eddy effects on the subduction of North Pacific mode waters. *Journal of Geophysical Research: Oceans*, *119*, 4867–4886. https://doi.org/10.1002/2014JC009861

Yeh, S.-W., Yi, D.-W., Sung, M.-K., & Kim, Y. H. (2018). An eastward shift of the North Pacific Oscillation after the mid-1990s and its relationship with ENSO. *Geophysical Research Letters*, *45*, 6654–6660. https://doi.org/10.1029/2018GL078671